Journal of Solid State Chemistry 181 (2008) 3151–3162

Contents lists available at ScienceDirect

Journal of Solid State Chemistry

journal homepage: www.elsevier.com/locate/jssc

High-temperature FeS–FeS_2 solid-state transitions: Reactions of solid mackinawite with gaseous H_2S

Y. Li, R.A. van Santen, Th. Weber *

Schuit Institute of Catalysis, Eindhoven University of Technology, 5600 MB Eindhoven, The Netherlands

ARTICLE INFO

Article history:
Received 3 January 2008
Received in revised form
31 July 2008
Accepted 17 August 2008
Available online 28 August 2008

Keywords:
Phase transitions
Iron sulfides
Mackinawite

ABSTRACT

Phase transitions and reactions of non-oxidized and surface-oxidized mackinawite (FeS) in helium and H_2S gas were investigated by means of X-ray diffraction (XRD), X-ray photoelectron spectroscopy (XPS) and density functional theory (DFT). DFT was used to obtain optimized structures of the iron–sulfur phases mackinawite, hexagonal pyrrhotite, greigite, marcasite and pyrite and to determine the thermochemical properties of reactions of mackinawite with H_2S to these phases. The phase transitions of mackinawite to hexagonal pyrrhotite are endothermic, while reactions to greigite, marcasite and pyrite are exothermic. The experiments show that non-oxidized mackinawite converts into hexagonal pyrrhotite (Fe_9S_{10} first and then Fe_7S_8) in He and also in H_2S but at a lower temperature. No further reactions can be observed under these conditions. In the case of surface-oxidized mackinawite, the extent of surface oxidation determines the course and the final product of the reaction with H_2S. If the extent of surface oxidation is low, only Fe^{2+} is oxidized to Fe^{3+}. Under these conditions mackinawite converts into the mixed-valence thiospinel compound greigite. In case of pronounced surface oxidation all surface Fe centers are oxidized to the Fe^{3+} state and S^{2-} is oxidized to SO_4^{2-}. Oxidation of sulfur is a prerequisite for the formation of pyrite.

1. Introduction

Transition metal sulfides are an important class of compounds. They show a variety of unusual structural and electronic properties and are of general significance for bio-, geo- and electrochemistry as well as catalysis. Iron sulfides constitute a wide-spread and diverse group of solids that play key roles in marine systems and in biogeochemistry. The evolution of the global biogeochemical sulfur cycle, for instance, is a major aspect of the evolution of the earth because the sulfur cycle is intimately involved in the cycles of a number of key elements including oxygen and carbon. Because of their role in the iron cycle, iron sulfides also provide information about the biogeochemistry of metals and are thus central to our understanding of the evolution of the earth [1,2].

Iron sulfides also play an important role in the iron–sulfur world hypothesis on the origin of life on earth [3–6], in which all of life's essential biomolecules are manufactured from small building blocks, such as H_2O, CO_2, H_2S and NH_3 (for a recent overview see Ref. [7]). In the model propagated by Wächtershäuser, the source of energy is the exothermic formation of the mineral pyrite (FeS_2) in the deep sea in either sedimentary systems from amorphous FeS [8], or in hydrothermal systems from amorphous FeS or pyrrhotite [9]. Both FeS-type phases are unstable with respect to the surrounding seawater and react with H_2S of volcanic origin to pyrite according to

$$FeS + H_2S \rightarrow FeS_2 + H_2 \quad (1)$$

Drobner et al. [10] modeled this reaction and concluded that it might proceed in two steps:

$$FeS + H_2S \rightarrow Fe(SH)_2 \quad (2)$$

$$Fe(SH)_2 \rightarrow FeS_2 + H_2 \quad (3)$$

Our interest in the FeS–FeS_2 transition was inspired by the question if it could be used within heterogeneous reactions for the generation of H_2 in industrial applications. For this purpose we have chosen mackinawite (FeS) as starting material and investigated reactions of mackinawite with H_2S by means of diffraction, spectroscopy and quantum chemical methods. Most of the published investigations related to FeS–FeS_2 phase transitions are conducted in solution. Here, the transformation of mackinawite to the more stable pyrite phase generally requires the presence of electron acceptors, such as dissolved low-valent sulfur species. Such species (e.g. polysulfide, sulfite, thiosulfate) are typically generated by incomplete oxidation of dissolved sulfide or

* Corresponding author. Present address: Shell Research and Technology Centre Amsterdam, Shell Global Solutions International B.V., Badhuisweg 3, NL-1031 CM Amsterdam, The Netherlands.
E-mail address: thomas.t.weber@shell.com (Th. Weber).

0022-4596/$ - see front matter © 2008 Elsevier Inc. All rights reserved.
doi:10.1016/j.jssc.2008.08.024

by dissolution of elemental sulfur [11]. Subsequent reaction of one or more of the oxidation products with mackinawite leads to the formation of the thiospinel compound greigite, which was in many cases found to be an intermediate phase in the conversion of mackinawite into pyrite [12]. For FeS–FeS_2 phase transitions within heterogeneous reactions nothing has been reported so far, which led Rickard and Luther to conclude that FeS–FeS_2 phase transitions are chemically unlikely under such reaction conditions [1].

In the present manuscript we describe the results of our investigation of the sulfidation of mackinawite in the absence and presence of electron acceptors. Sulfidation is a well-known procedure in the preparation of molybdenum and tungsten-based hydrotreating catalysts and refers to the generation of active sulfide catalysts by reaction of solid precursor materials with gaseous H_2S or gas mixtures containing H_2S [13,14]. We have introduced electron acceptors to our reaction system in the form of oxidized surface species formed within reactions of freshly prepared mackinawite with synthetic air under controlled conditions. In order to be able to distinguish between phase transitions of mackinawite and sulfidation processes we have also studied the behavior of FeS in inert gas upon thermal treatment.

2. Experimental and computational details

2.1. Synthesis of mackinawite

Mackinawite was synthesized in analogy to published methods [15] under carefully controlled oxygen-free conditions using a Schlenk setup. First, 12.6 g $(NH_4)_2Fe(SO_4)_2$ and 7.1 g Na_2S were filled in separate Schlenk bottles. The bottles were three times evacuated and subsequently flushed with Ar. Then 200 ml of degassed water were added to each bottle with a syringe under protection with Ar. After the solids were entirely dissolved, the solutions were combined by drop wise adding the Na_2S solution to the $(NH_4)_2Fe(SO_4)_2$ solution under stirring. A black material precipitated immediately. The mixture was stirred for 2 h, filtrated with a Schlenk filter (Whatman, no. 4) and the solid product was washed three times with degassed water and ethanol. The product was dried overnight in vacuum and stored in an N_2-operated glove box. The nitrogen used for this purpose was of high purity and additionally post-purified. It contained residua of O_2 and H_2O together of less than 1 ppm.

2.2. Oxidation of mackinawite

Freshly prepared mackinawite is highly sensitive to air and can even be pyrophoric (ignite spontaneously). Direct expose of mackinawite to air leads to full oxidation of its surface. For oxidizing the surface in a reproducible and controlled way we have used the following procedure: the surface of the freshly prepared sample was first passivated in an atmosphere that contains very low concentrations of O_2 by storing the sample overnight in a reactor that contained between 3 and 5 ppm of O_2 in N_2. The surface passivated samples were then transferred into a quartz reactor in which they were exposed to synthetic air consisting of 5% O_2 in He for different periods of time (between 2 min and 12 h). Preoxidized samples were stored in sealed bottles in the N_2-operated glove box.

2.3. Thermal treatment of mackinawite with H_2S or He

The reactions of mackinawite with H_2S or He were carried out in a quartz reactor, which was transferred into the glove box for loading and unloading the samples. The reactor was filled with ca. 100 mg mackinawite, closed, connected to the gas supply and purged with either He or a 9.9 vol% H_2S/Ar gas mixture. The solid was heated from room temperature to the desired temperature at a rate of 2 °C/min in 15 ml/min gas flow, kept at this temperature for given periods of time and then cooled down in a He flow. After reaction, the reactor was closed. The sample was transferred to a bottle and stored in the glove box.

2.4. Characterization methods

X-ray diffraction (XRD) powder diffraction patterns from $2\theta = 10^\circ$ to 80° were measured with a Rigaku D/Max diffractometer using Cu $K\alpha$ radiation ($\lambda = 1.5406$ Å). The samples were measured as a paraffin mull on a glass holder under ambient conditions. *In situ* XRD measurements were done with a PANalytical X'pert system equipped with an Anton Parr XRD controlled atmosphere measuring cell. Mounting the sample in the measuring cell was done in a glove box. The prepared cell was purged with argon, heated to the desired temperature at a heating rate of 2 °C/min and kept at each temperature for 5 min before the measurements were started.

X-ray photoelectron spectroscopy (XPS) spectra were measured with a VG Escalab 200 MK spectrometer equipped with an Al $K\alpha$ source and a hemispherical analyzer connected to a five-channel detector. During measurement the base pressure of the system was around 2.0×10^{-9} bar. Spectra were recorded at constant pass energy of 20 eV. Charging was corrected for the C 1 s signal at 284.5 eV. Computer fitting of the measured spectra was used to derive the binding energies. Binding energies are estimated to be accurate within ± 0.3 eV.

The samples were pressed into carbon foil for the measurements. All the preparation steps were carried out under inert conditions. Transfer of the samples from the reactors to the UHV chamber of the spectrometer was done by using a nitrogen-operated glove box and a special inert gas transport vessel.

2.5. DFT calculations

Density functional theory (DFT) calculations were performed with the Accelrys Materials Studio 4.0 software package applying the DMol^3 [16,17] and Castep [18] codes with a double-numeric polarized basis set and a medium level of integration grid consisting of approximately 1000 grid points per atom. The non-local exchange-correlation functional of Perdew and Wang (PW91) was applied [19]. We used ultra-soft pseudo-potentials in the Castep calculations and semi-core pseudo-potentials or an all-electron core-treatment in the DMol^3 calculations. The structures of the Fe–S phases were generated from X-ray crystallographic data. Spin states of Fe atoms were explicitly set and spin polarization was taken into consideration.

3. Results

The organization of this section is as follows: we will first describe the results of the quantum chemical calculations, which are used to determine the thermochemical profile of the reactions of mackinawite with H_2S to other Fe–S solid-state phases. Next we will present the characterization of mackinawite (non-oxidized and surface-oxidized) and then describe phase transitions of mackinawite upon heating in He atmosphere as well as reactions with gaseous H_2S. Oxidation of mackinawite changes the surface states of iron and sulfur so that the resulting surface bears similarities with that of iron(III) sulfate. Boursiquot et al. showed

that after exposure to air for several weeks, mackinawite decomposes into elemental sulfur and different iron(III) oxides [20]. Therefore, we also studied the sulfidation of $Fe_2(SO_4)_3$ and Fe_2O_3 (hematite) as model reactions.

3.1. DFT calculations

We calculated the thermochemical properties of the two types of gas-phase reactions:

$$FeS + x\tfrac{1}{8}S_8 \rightarrow FeS_{1+x} \quad (4)$$

and

$$FeS + xH_2S \rightarrow FeS_{1+x} + xH_2 \quad (5)$$

in the range $0 \leqslant x \leqslant 1$. In the calculations we considered reactions of mackinawite [21] to hexagonal pyrrhotite (Fe_9S_{10} [22,23] and Fe_7S_8 [24]), greigite (Fe_3S_4) [25], marcasite (FeS_2) [26] and pyrite (FeS_2) [27]. Crystallographic specifications are compiled in Table 1. For determining the thermochemical profile of reaction (4) we first calculated the energies of the different phases by performing a full geometrical relaxation and then referencing the energy of the respective compound (FeS_{1+x}) to that of mackinawite and elemental sulfur ($FeS + x\frac{1}{8}S_8$). For reaction (5) the exothermic energy gain of the formation of H_2S from H_2 and elemental sulfur is considered. The calculated results for reactions (4) and (5) are listed in Table 2. All three computational methods, i.e. ultra-soft and semi-core pseudo-potentials as well as all-electron calculations, gave comparable trends for the reactions of mackinawite with either elemental sulfur or H_2S to pyrrhotite, greigite, marcasite and pyrite. In contrast to thermodynamical data obtained from solution chemistry [28], marcasite was reproducibly calculated slightly more stable than pyrite. A phase that requires a deeper inspection is the mixed-valence Fe^{II}/Fe^{III} thiospinel compound greigite. All our calculations describe the formation of greigite as exothermic with respect to mackinawite, which is in line with structural chemical considerations (*vide infra*). The extent of exothermicity, however, differs among the two DFT codes. The semi-core pseudo-potential as well as the all-electron calculations (DMol^3) give very high stabilities (around −40 kcal/mol), whereas the ultra-soft pseudo-potential calculations (Castep) lead to energy values close to those of marcasite and pyrite (around −20 kcal/mol). This difference arises most likely from how the DFT codes account for the magnetic properties of the thiospinel structure. The converged results of the DMol^3 calculations imply ferrimagnetic behavior, which might account for the rather low energy. It is known that DFT calculations of magnetic transition–metal sulfides are critical [29,30] and can lead to results (structure, cell volume, bond length, energy) that may differ significantly from experimental findings. In view of the evaluation of computational settings as discussed in Ref. [29] we tend to rely more on the results of the ultra-soft pseudo-potential calculations as obtained with the Castep code. The thermochemical profile of reaction (5) is shown in Fig. 1.

Our calculations lead to the following general conclusions: The overall reaction of mackinawite with gaseous H_2S to pyrite is exothermic by -16 ± 3 kcal/mol. The reactions of mackinawite to hexagonal pyrrhotite are endothermic by 13 ± 3 kcal/mol (Fe_9S_{10}) and 11 ± 3 kcal/mol (Fe_7S_8), while the formation of greigite is exothermic by 19 ± 3 kcal/mol.

Table 1
Cystallographic data of the calculated Fe–S compounds

Compound	Formula	Space group	*a*	*b*	*c*
Mackinawite	FeS (FeS_{1-x})	*P4/nmm* (129)	3.673	3.673	5.032
Pyrrhotite, hexagonal	FeS	$Cmc2_1$ (36)	10.856	6.268	5.034
Pyrrhotite, monoclinic	$FeS_{1.1429}$	$P3_121$ (152)	6.866	6.866	17.088
Greigite	$FeS_{1.333}$	$Fd\bar{3}m$ (227)	9.876	9.876	9.876
Marcasite	FeS_2	*Pnnm* (58)	4.443	5.424	3.386
Pyrite	FeS_2	$Pca2_1$ (29)	5.417	5.417	5.417

Lattice parameters *a*, *b* and *c* are in Å.

Table 2
Thermochemical data for the formation of FeS_{1+x} compounds ($0 < x \leqslant 1$) by reaction of FeS (mackinawite) with elemental sulfur (reaction 4) or H_2S (reaction 5) as obtained with (a) all-electron (DMol^3), (b) semi-core pseudo-potential (DMol^3) and (c) ultra-soft pseudo-potential DFT calculations (Castep)

Compound	$FeS + x\frac{1}{8}S_8 \rightarrow FeS_{1+x}$			$FeS + xH_2S \rightarrow FeS_{1+x} + xH_2$		
	a	*b*	*c*	*a*	*b*	*c*
Pyrrhotite $FeS_{1.111}$	10	12	15	11	13	16
Pyrrhotite $FeS_{1.1423}$	8	9	13	9	10	14
Greigite $FeS_{1.333}$	−41	−41	−21	−39	−39	−19
Marcasite FeS_2	−25	−26	−20	−18	−20	−13
Pyrite FeS_2	−24	−25	−19	−17	−18	−12

Energy values are in kcal/mol.

3.2. Mackinawite and surface-oxidized mackinawite

We prepared mackinawite by precipitation from aqueous solution at room temperature in analogy to the procedure published by Ohfuji and Rickard [15]. Under these conditions mackinawite forms as particles with a sheet-like morphology and a size of about several hundred nanometers. Due to the small particles the XRD pattern (not shown) consists of only rather broad features and this material was referred to as amorphous or poorly ordered FeS in earlier studies [15,31,32]. We have chosen to use this material rather than well-defined crystals, because we are interested in the heterogeneous reaction of solid mackinawite with gaseous H_2S, which proceeds kinetically easier in the case of small particles.

The effect of oxidation on the state of the mackinawite surface is demonstrated by the XPS spectra shown in Fig. 2; binding energies are compiled in Table 3. Due to the high sensitivity of the mackinawite surface towards reaction with even traces of O_2, partial oxidation of the surface is very difficult to avoid. This is reflected in the XPS spectra of the freshly prepared mackinawite sample (spectra I in Figs. 2a–c). The S 2*p* XPS signal is composed of two doublets with S $2p_{3/2}$ components at 161.7 ± 0.3 and 163.6 ± 0.3 eV. The binding energy of the major doublet (90%) at 161.7 ± 0.3 eV is typical of S^{2-} species [33,34]. The second minor doublet (10%) is located at 163.6 ± 0.3 eV and is due to sulfur species in higher formal oxidation states than −2, such as in polysulfide ligands (S_n^{2-}) and elemental sulfur. The Fe 2*p* XPS spectrum of mackinawite (Fig. 2b) is rather broad and is composed of three doublets. The weak O 1*s* peak (Fig. 2c) shows that partial oxidation of the surface has taken place. For this reason we are considering iron to be present as Fe^{II} and Fe^{III} in sulfidic and oxidic environments. We assign the three components in the following way: 707.1 ± 0.3 eV: Fe^{II}–S (82%), 709.2 ± 0.3 eV: Fe^{III}–S (16%) and 711.5 ± 0.3 eV: Fe^{III}–O (2%). The presence of Fe^{II} and Fe^{III} on the mackinawite surface was also found by Mullet et al. [35]. Oxidizing the mackinawite surface changes the appearance of the XPS spectra significantly. While the S 2*p* XPS signal of freshly prepared mackinawite consists of two doublets only, two more contributions to the overall envelope become visible during oxidation, one at 162.3 ± 0.3 eV after 2 min of

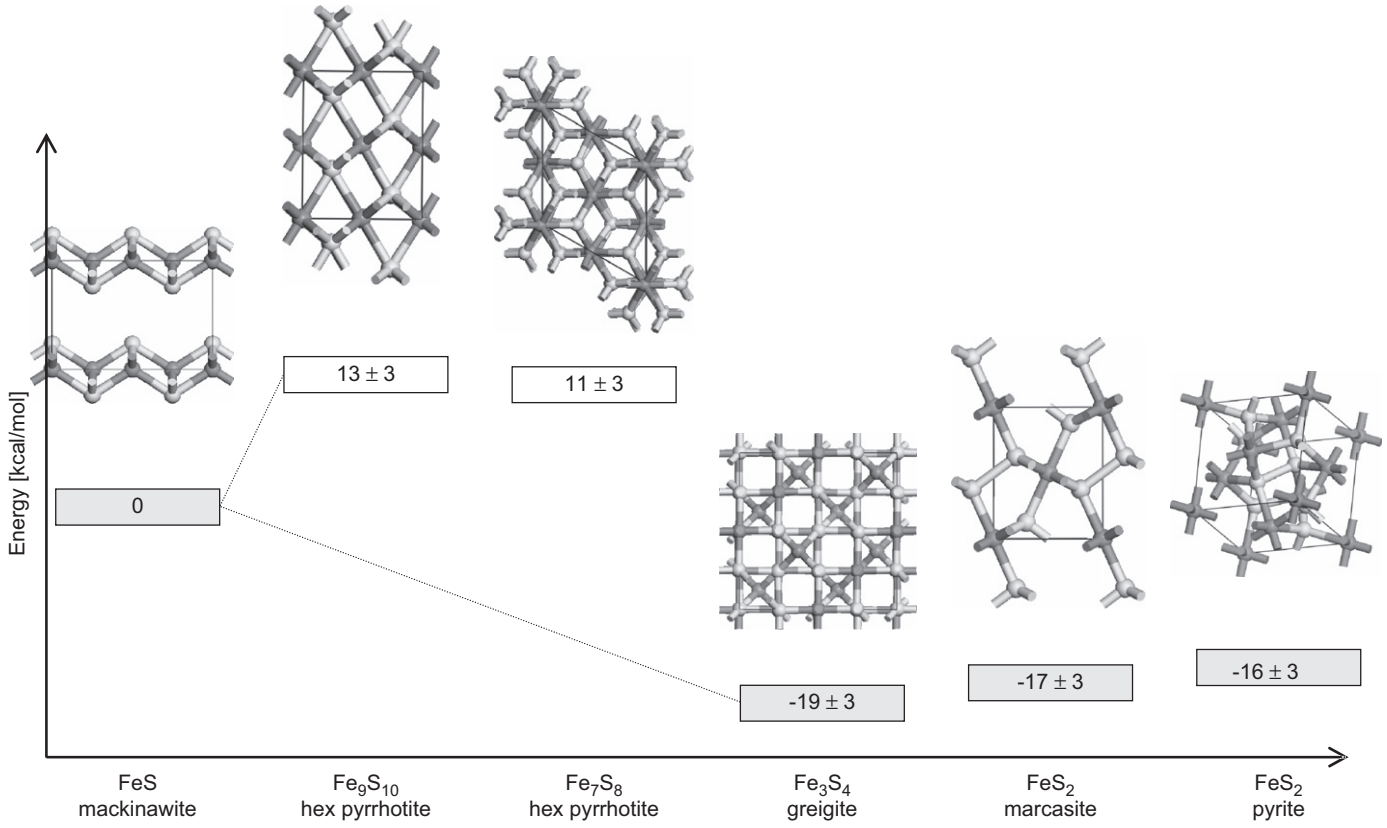

Fig. 1. Thermochemical properties of the reaction of mackinawite with H_2S to different Fe–S phases.

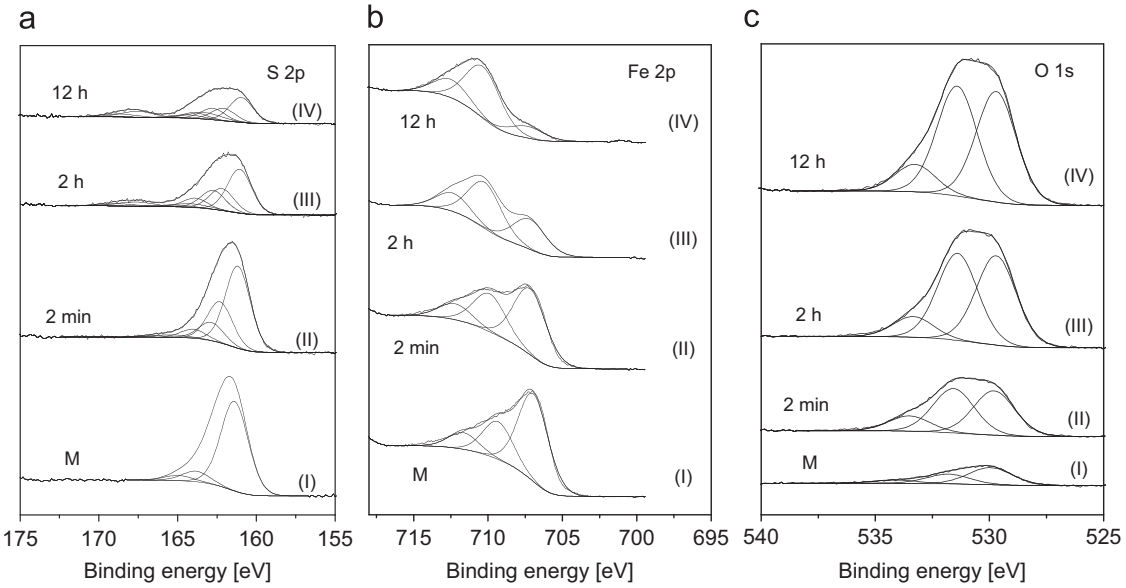

Fig. 2. Fe 2*p*, S 2*p* and O 1*s* XPS spectra of freshly prepared mackinawite and after exposure to synthetic air (5% O_2 in He) for 2 min, 2 and 12 h.

oxidation and another at 168.0 ± 0.3 eV after 2 h of oxidation. These signals point to the presence of disulfide (S_2^{2-}, 162.3 ± 0.3 eV) and sulfate surface species (SO_4^{2-}, 168.0 ± 0.3 eV). As in the case of the freshly prepared mackinawite, the Fe 2*p* spectra of the oxidized samples are composed of three contributions, which however, undergo shifts to higher binding energies, as the respective contributions of the S 2*p* signal also shift to lower binding energies (see Table 3). The XPS spectra clearly show that surface Fe centers are primarily affected by oxidation, i.e. Fe^{2+} is oxidized to Fe $^{3+}$. If all—or at least most—of the iron is oxidized, only then further treatment with O_2 leads to oxidation of S^{2-} on the surface of the sample to SO_4^{2-}. This sequence can clearly be identified by comparing spectra (III) and (IV) in Figs. 2a and b.

3.3. Reactions of non-oxidized mackinawite

3.3.1. Thermal treatment

Fig. 3 shows the XRD patterns and XPS spectra of freshly prepared, non-oxidized mackinawite after treatment in He gas at 150, 200 and 300 °C for 3 h, respectively. The XRD measurements show that mackinawite transforms gradually into pyrrhotite. The XRD pattern of the sample after treatment at 150 °C shows the reflections of mackinawite more clearly than the freshly prepared material does, which points to crystallization as the first process to take place. At 200 °C mackinawite converts into pyrrhotite. The term "pyrrhotite" encompasses a series of phases with different structures, superstructures and stoichiometries. The reflections in the XRD pattern of the sample after thermal treatment at 200 °C are characteristic of hexagonal pyrrhotite (Fe_9S_{10}), which is the first reaction intermediate of mackinawite. Further heating to 300 °C leads to a second phase transition, during which Fe_7S_8, another hexagonal pyrrhotite phase forms as demonstrated by XRD (Fig. 3a).

Figs. 3b and c show the corresponding S 2*p* and Fe 2*p* XPS spectra; XPS binding energies are listed in Table 4 (upper part) together with XRD phase compositions. The spectra obtained after treating mackinawite at 150 and 200 °C are virtually identical. The spectrum of the sample treated at 300 °C, however, shows shifts of the Fe 2*p* and S 2*p* signals in opposite directions. While the S 2*p* signal shifts to lower binding energy by ca. 0.7 eV, the Fe 2*p* signal shifts to higher binding energy by 0.5 eV.

Our XRD and XPS measurements of the thermal treatment of mackinawite in inert gas lead to the following conclusions: mackinawite is stable to above 150 °C. In this temperature interval crystallization is the only process that takes place. Close to

Table 3
Binding energies in the S 2*p* and Fe 2*p* XPS spectra of freshly prepared mackinawite and after exposure to synthetic air as shown in Fig. 2

Species	Mackinawite	2 min	2 h	12 h
S^{2-}	161.7	161.4	161.3	161.1
S_2^{2-}		162.3	162.1	162.1
S_0/S_n^{2-}	163.6	≈163.3	≈163.6	≈163.6
SO_4^{2-}			168.0	168.0
Fe^{II}–S	707.1	707.1	707.1	707.1
Fe^{III}–S	709.2	709.7	710.1	710.3
Fe^{III}–O	711.5	712.2	712.4	712.5

Binding energies are accurate within ±0.3 eV.

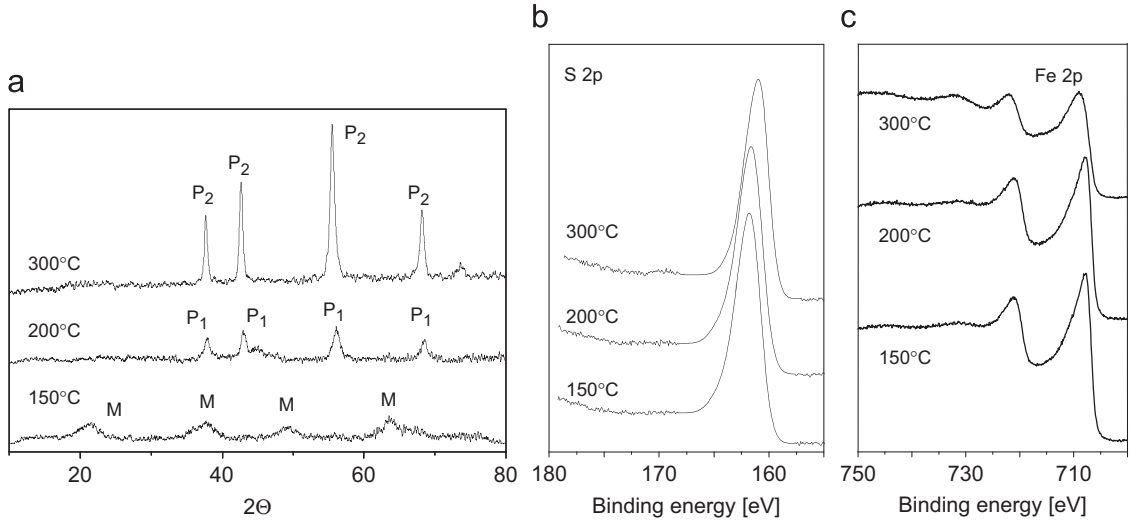

Fig. 3. XRD patterns (a) and XPS spectra (b, c) of non-oxidized mackinawite after thermal treatment in He (M: mackinawite, P_1: Fe_9S_{10}, P_2: Fe_7S_8).

Table 4
Binding energies (BE) of the S 2*p* and Fe $2p_{3/2}$ XPS spectra and phase compositions as obtained by XRD analysis of the time- and temperature-dependent treatments of mackinawite with He (upper part) or H_2S gas (lower part)

Experimental conditions			BE (eV)		XPS	XRD
Gas	*T* (°C)	*t* (h)	Fe 2*p*	S 2*p*	S/Fe	phase composition
	Mackinawite		706.6	161.5	0.84	M
He	150	3	706.8	161.7	0.85	M
He	200	3	706.7	161.5	0.87	P_9
He	300	3	707.2	160.9	1.22	P_7
H_2S	100	3	706.8	161.7	0.92	M
H_2S	150	1	706.5	161.4	0.93	M
H_2S	150	3	706.6	161.6	0.96	M
H_2S	150	6	706.9	161.3	1.04	M+P_9
H_2S	150	12	707.1	160.9	1.25	M+P_9
H_2S	200	3	707.4	161.1	1.15	P_7
H_2S	250	3	707.2	160.9	1.27	P_7
H_2S	300	3	707.4	161.0	1.24	P_{70}

Binding energies are accurate within ± 0.3 eV. M: mackinawite, P_9: Fe_9S_{10}, P_7: Fe_7S_8.

200 °C the microcrystalline mackinawite converts into hexagonal pyrrhotite (Fe_9S_{10}), which undergoes a phase transition to Fe_7S_8 between 250 and 300 °C. XPS spectra of mackinawite and Fe_9S_{10} are virtual identical and contain contributions that can reasonably well be explained with the presence of Fe^{II} centers and S^{2-} ligands. The phase transition to the hexagonal pyrrhotite phase Fe_7S_8 changes the appearance of the XPS spectrum by shifts of the Fe 2*p* and S 2*p* signals into opposite directions.

3.3.2. *Reaction with H_2S*

Figs. 4a and b show the XRD patterns of the temperature- and time-dependent reactions of mackinawite with H_2S. As in the case of the thermal treatment in He, the XRD patterns reflect the gradual change of mackinawite to pyrrhotite but with clear differences. The XRD pattern obtained after reaction at 150 °C (Fig. 4a) shows that the sample is less crystalline than it was under the same conditions in He atmosphere (Fig. 3a). The phase transition of mackinawite to hexagonal pyrrhotite (Fe_9S_{10}) takes already place at 150 °C (Fig. 4b). After 6 h at 150 °C XRD clearly shows the presence of Fe_9S_{10}, which undergoes further structural ordering upon prolonged heating. We were never able to observe any phase transitions of mackinawite at 150 °C in He atmosphere. According to XRD, mackinawite is fully transformed into the hexagonal pyrrhotite phase Fe_9S_{10} at 200 °C. Heating the sample to 300 °C induces the bulk transition to Fe_7S_8, which seems to take place in a similar way as in He. These findings show that the phase transition of mackinawite to Fe_9S_{10} in H_2S is different from that in He, because it takes place at significantly lower temperature in H_2S. While in He further reactions of the eventually formed pyrrhotite to Fe–S phases of higher S:Fe stoichiometries, such as pyrite, cannot take place due to a missing source of sulfur, such reaction would in principle be possible in H_2S atmosphere. With non-oxidized mackinawite, however, we did not observe reactions of pyrrhotite to pyrite.

Figs. 4c and d show the XPS spectra of the temperature- and time-dependent reactions of mackinawite with H_2S; XPS binding energies and XRD phase compositions are listed in Table 4 (lower part). While the XRD measurements showed that the transition of mackinawite to hexagonal pyrrhotite (Fe_9S_{10}) proceeds in H_2S atmosphere already at 150 °C after 6 h of reaction time, the XPS data point to another interesting difference of the reactivity of mackinawite in H_2S gas compared to inert gas. As already mentioned, the XPS spectra of mackinawite and hexagonal pyrrhotite are virtually identical. This can be recognized within the experimental accuracy of ± 0.3 eV in Fig. 4d up to a reaction time of 6 h. After 12 h, however, the S 2*p* and Fe 2*p* signals undergo shifts into opposite directions (S 2*p*: −0.5 eV, Fe 2*p*: +0.4 eV), similarly as we observed it for the phase transition from Fe_9S_{10} to Fe_7S_8 (*vide supra*). Together with the increase of the XPS S/Fe ratio,

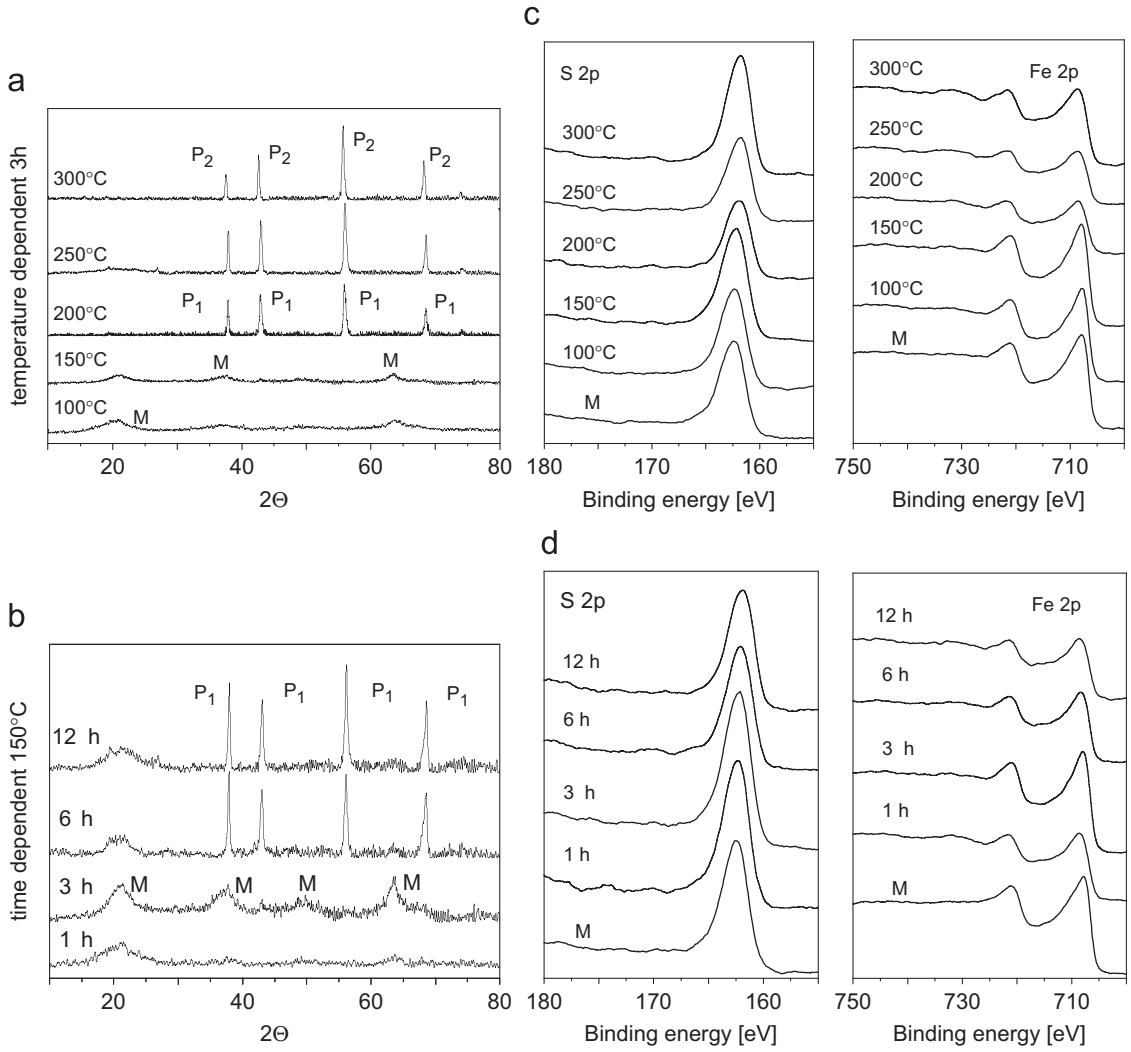

Fig. 4. XRD patterns (a, b) and XPS spectra (c, d) of non-oxidized mackinawite after reaction with H_2S at different temperatures for 3 h, (a, c) and for different periods of time at 150 °C (b, d). M: mackinawite, P_1: Fe_9S_{10}, P_2: Fe_7S_8.

we conclude that after 12 h at 150 °C in H_2S the surface of the sample has undergone partial transition to Fe_7S_8. This finding again points to the different chemistry involved in the phase transitions in the presence of H_2S. In the case of the temperature-dependent reaction of mackinawite with H_2S, the changes of the S 2*p* peak position undergo a similar trend as in the case of the time-dependent reaction at 150 °C, i.e. the signal shifts gradually to lower binding energies. At 300 °C the S 2*p* XPS signal consists of two components, the main component (≈80%) at 160.6±0.3 eV and an additional component (≈20%) at 162.8±0.3 eV, the latter being typical of S_2^{2-} ligands in bridging coordination types [36].

Our XRD and XPS investigations of the time- and temperature-dependent reactions of mackinawite in H_2S can be summarized as follows: as in the case of the thermal treatment in He atmosphere, mackinawite transforms first into the hexagonal pyrrhotite phase Fe_9S_{10} and then into Fe_7S_8, which is the final product; no further reaction to phases with higher S:Fe stoichiometries are observed. All steps, however, are taking place at lower temperatures as in He. The transition of mackinawite to hexagonal pyrrhotite takes already place at 150 °C. After 12 h at 150 °C the surface of the sample partly converted into hexagonal pyrrhotite, while for the full bulk conversion temperatures above 200 °C are required.

3.4. Reactions of solid surface-oxidized mackinawite

3.4.1. Thermal treatment

Phase transitions of mackinawite in inert gas atmosphere were investigated by means of *in situ* XRD measurements. Fig. 5 shows the XRD patterns of a mackinawite sample that was surface oxidized for 2 min in synthetic air (lower trace in Fig. 5a) and after treating the sample in argon at different temperatures. The diffraction patterns demonstrate that mackinawite converts via greigite as intermediate phase into pyrrhotite (Fe_7S_8). Reflections of mackinawite are visible in the powder patterns up to 150 °C, while characteristic features of greigite start to emerge at 120 °C. According to XRD, a full conversion of mackinawite to greigite has taken place at 170 °C. Greigite is stable up to 230 °C (Fig. 5b) and transforms then upon further heating to 500 °C into a well-defined pyrrhotite phase, which is the main constituent above 290 °C. In conclusion, the mackinawite–greigite conversion takes place between 120 and 170 °C, while the greigite–pyrrhotite transition occurs between 230 and 290 °C. Greigite is thus stable between 170 and 230 °C and pyrrhotite above 290 °C.

3.4.2. Reaction with H_2S

3.4.2.1. Effect of surface oxidation. The effect of surface oxidation on the course of the reaction of mackinawite with H_2S can be seen in Fig. 6, which shows XRD patterns (Fig. 6a) and XPS spectra (Figs. 6b–d) of mackinawite samples that were oxidized in synthetic air for 2 min or 2 h and then sulfided for 3 h at 300 °C (traces I and II) and of a sample that was first surface oxidized in synthetic air for 2 min and sulfided (3 h, 300 °C) then again oxidized in synthetic air for 2 min and resulfided (III). The XRD patterns in Fig. 6a clearly show that in all cases the starting material mackinawite has transformed into other Fe–S phases. This is not surprising because the sulfidation temperature (300 °C) lies above the stability range of mackinawite. In the case of minor surface oxidation (2 min), mackinawite transforms into a mixture of greigite and pyrrhotite (pattern I, Fig. 6a), while a mixture of pyrrhotite and pyrite forms with the 2 h preoxidized sample (pattern II, Fig. 6a). Before reoxidation and resulfidation sample (III) is in the same state as sample (I), i.e. a mixture of greigite and pyrrhotite. Exposing this mixture to synthetic air for 2 min and subsequent sulfidation converts the mixture into pyrite (pattern III, Fig. 6a).

The respective XPS spectra (binding energies are listed in Table 5) are less conclusive than the XRD patterns. Obviously the sulfidation products contain more surface species than it is expected on the basis of their XRD bulk compositions. This is due to surface oxidation, which can be seen from the O 1*s* XPS spectra (Fig. 6d). The XPS spectrum of sample (III) is rather close to its expected appearance. According to XRD the sample consists of pyrite, which is composed of Fe^{II} and S_2^{2-} and, in agreement with this, corresponding S 2*p* and Fe 2*p* signals at 162.3±0.3 and 707.1±0.3 eV constitute the main components of the respective XPS spectra. A weak feature at 168.6±0.3 eV in the S 2*p* spectrum points to the presence of highly oxidized surface species, such as SO_4^{2-}. The Fe 2*p* XPS spectra of the sample oxidized for 2 min and then sulfided (trace I, Fig. 6c) is composed of two contributions at 707.3±0.3 and 711.8±0.3 eV, which can clearly be assigned to Fe^{II}–S and Fe^{III}–S in line with the XRD bulk composition (greigite and pyrrhotite). The S 2*p* XPS spectrum consists of mainly contributions due to S^{2-} (160.9±0.3 eV) and to a much lesser extent S_2^{2-} (162.5±0.3 eV), but also of a weak feature at 164.2±0.3 eV, which indicates the presence of small amounts of polysulfide surface groups. Interestingly the XPS spectra of this sample are very similar to those of the respective unsulfided sample (Fig. 2). Sample (II) is according to XRD a

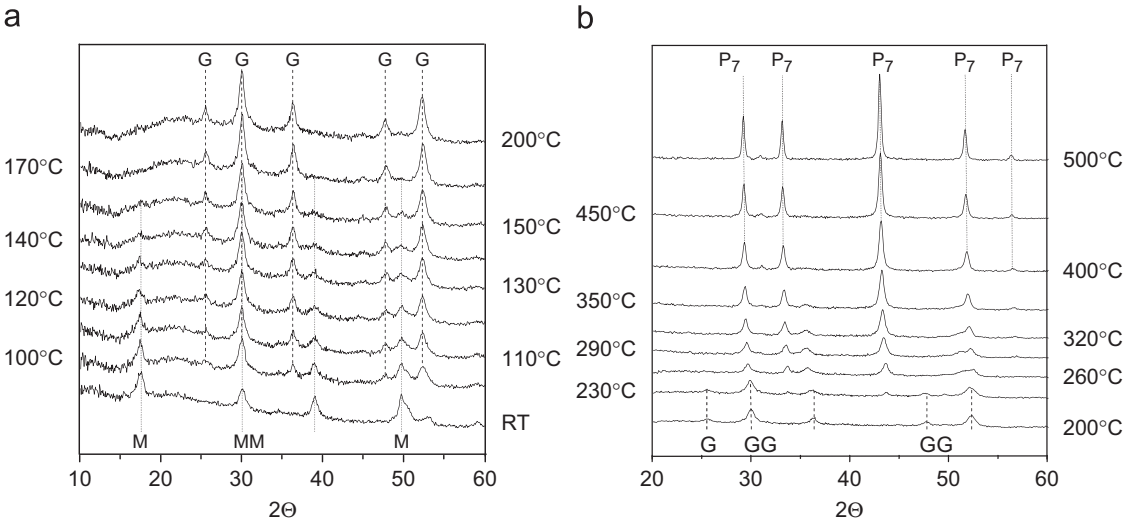

Fig. 5. *In situ* XRD patterns of mackinawite obtained in Ar atmosphere at given temperatures. M: mackinawite, G: greigite, P_7: pyrrhotite (Fe_7S_8).

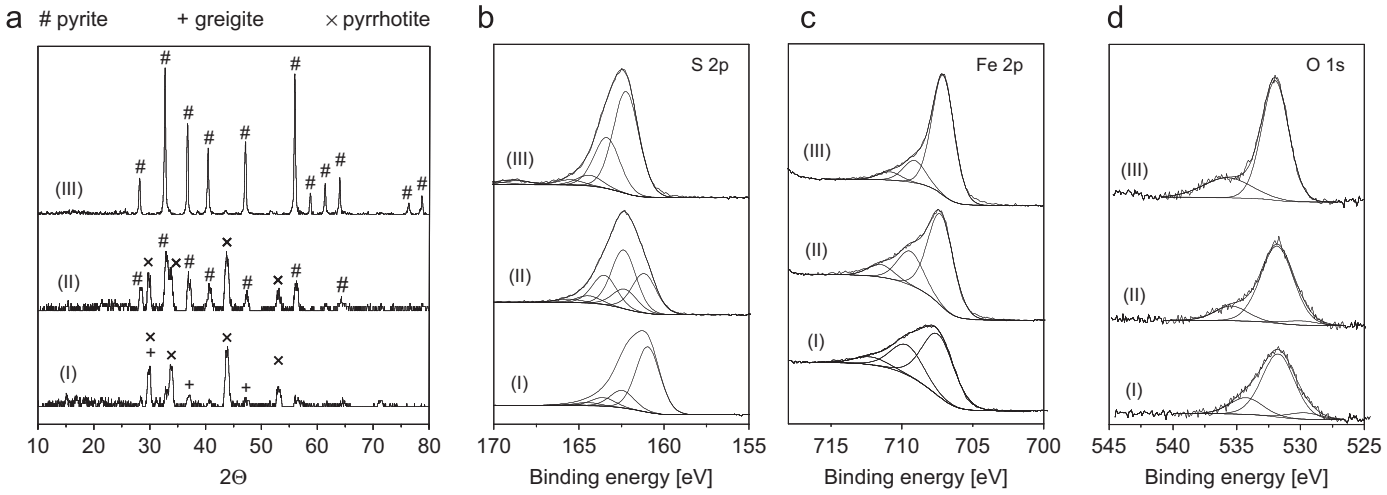

Fig. 6. XRD patterns (a) and Fe 2*p*, S 2*p* and O 1*s* XPS spectra (b–d) of mackinawite samples, which were exposed to synthetic air for 2 min (I) or 2 h (II) and then sulfided for 3 h at 300 °C. Pattern (III) and spectra (III) were obtained from a sample treated like (I), then reexposed to synthetic air for 2 min and again sulfided for 3 h at 300 °C.

Table 5
Binding energies in the S 2*p* and Fe 2*p* XPS spectra shown in Figs. 6b–d

Species	(I)	(II)	(III)
S^{2-}	160.9	161.1	
S_2^{2-}	162.5	162.4	162.3
S_0/S_n^{2-}	164.2	164.5	164.5
SO_4^{2-}			168.6
Fe^{II}–S	707.6	707.3	707.1
Fe^{III}–S	709.9	709.5	709.2
Fe^{III}–O	712.3	711.6	711.1

Binding energies are accurate within ±0.3 eV.

mixture of pyrrhotite and pyrite and thus the Fe 2*p* XPS spectra should mainly consist of a signal due to Fe^{II}–S species and the S 2*p* spectrum should be composed of two contributions due to the presence of S^{2-} and S_2^{2-}. This can indeed been seen in the respective XPS spectra (Fe 2*p*: 707.3±0.3; S 2*p*: 161.1±0.3 and 162.4±0.3 eV). The Fe 2*p* envelope, however, also contains a contribution due to Fe^{III}–S species at 709.5±0.3 eV. This observation is unexpected with respect to oxidation states of the constituents. However, the presence of both Fe^{II} and Fe^{III} coordinated to S^{2-} has been found for a variety of $Fe^{II}S^{2-}$-type phases, among them the constituents of sample (II), pyrrhotite [37] and pyrite [38] and also mackinawite [39].

The sulfidation reaction of surface-oxidized mackinawite samples with H_2S at 300 °C can be summarized as follows: mackinawite transforms in dependence of its state of surface oxidation into pyrite via greigite and pyrrhotite as intermediate phases. In the case of minor surface oxidation (2 min), a mixture of greigite and pyrrhotite forms upon sulfidation. Mackinawite that was oxidized under more severe conditions (2 h) reacts to a phase composed of pyrrhotite and pyrite. The greigite–pyrrhotite mixture, if again oxidized and sulfided, converts completely into pyrite. Obviously the amount of oxidized species available at the surface of the samples determines the course of the sulfidation reaction.

3.4.2.2. Effect of sulfidation time. The effect of sulfidation time on the course of the reaction of surface-oxidized mackinawite with H_2S can be seen in Fig. 7, which shows XRD patterns (Fig. 7a) and XPS spectra (Figs. 7b–d) of a mackinawite sample that was oxidized in synthetic air for 2 h and then sulfided at 150 °C for 1, 16 or 48 h; XPS binding energies are compiled in Table 6. Mackinawite is at least stable up to about 180 °C (see above and also Ref. [40]) so that all conversions observed upon sulfidation at 150 °C are mainly due to reaction with H_2S rather than to phase transitions or phase degradation processes. Again mackinawite converts gradually into pyrite with greigite and pyrrhotite as intermediate phases. The XRD pattern obtained after 1 h of sulfidation clearly indicates the presence of greigite as the main constituent, which also forms together with pyrrhotite during 16 h of sulfidation. After 48 h mackinawite has converted into a mixture of pyrrhotite and pyrite. A further increase of sulfidation time does not change the result.

Figs. 7b–d show the XPS spectra of the time-dependent sulfidation of the surface-oxidized mackinawite sample. According to XRD all obtained sulfidation products are mixtures of different phases so that this should be reflected in the XPS spectra as well. The products obtained after sulfidation for 1 or 16 h contain greigite, and it is thus reasonable that Fe 2*p* signals due to the presence of Fe^{2+} and Fe^{3+} are observed (signals at 707.9± 0.3 eV and 710±0.3 eV). In agreement with this assignment, an S $2p_{3/2}$ contribution around 161.5 eV due to S^{2-} forms the main component of the S 2*p* envelope. The phase obtained after sulfidation for 48 h is a mixture of pyrrhotite and pyrite and, correspondingly, signals due to the presence of Fe^{2+}, S^{2-} and S_2^{2-} are present in the respective XPS spectra (spectra III, Figs. 7b and c): 707.6±0.3 eV (Fe^{II}–S), 161.0±0.3 eV (S^{2-}) and 163.0± 0.3 eV (S_2^{2-}). As already mentioned in connection with the samples sulfided at 300 °C (Fig. 6) the number of surface species as detected by XPS is higher than expected on the basis of the XRD results. Sample (III) for instance does also contain small amounts of Fe^{III}–S groups, while the spectra of samples (I) and (II) show features due to the presence of S_2^{2-}.

Our investigation of the time-dependent sulfidation of a mackinawite sample oxidized for 2 h at 150 °C can be summarized as follows: regardless of the chosen reaction time, full conversion into pure pyrite cannot be observed. In all cases mixtures of Fe–S phases are formed.

3.5. Reactions of Fe_2O_3 and $Fe_2(So_4)_3$ with H_2S

The results of the sulfidation of Fe_2O_3 and $Fe_2(SO_4)_3$ are displayed in Fig. 8. The XRD patterns (Figs. 8a and b) show that

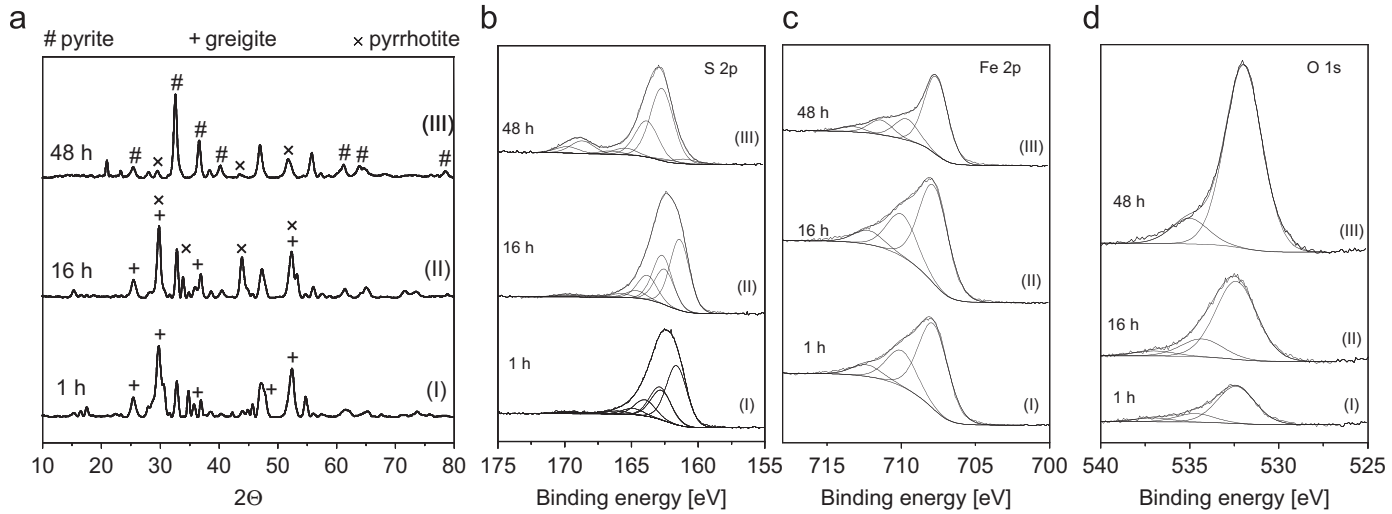

Fig. 7. XRD patterns (a) and Fe 2*p*, S 2*p* and O 1*s* XPS spectra (b–d) of preoxidized mackinawite (2 h in synthetic air) after reaction with H_2S at 150 °C for 1, 16 or 48 h.

Table 6
Binding energies in the S 2*p* and Fe 2*p* XPS spectra shown in Figs. 7b–d

Species	1 h	16 h	48 h
S^{2-}	161.7	161.4	161.0
S_2^{2-}	162.9	162.6	163.0
S_0/S_n^{2-}	164.9	164.6	165.1
SO_4^{2-}			168.2
Fe^{II}–S	707.9	707.9	707.6
Fe^{III}–S	710.1	710.0	709.7
Fe^{III}–O	712.3	712.3	711.5

Binding energies are accurate within ±0.3 eV.

both compounds, although chemically very different, convert into pyrite upon sulfidation at 300 °C for 6 h. The pyrite phase that forms during sulfidation of hematite is clearly better defined than that obtained by sulfidation of iron(III) sulfate. XPS spectra are shown in Figs. 8c–e; binding energies are listed in Table 7. The Fe 2*p* and S 2*p* XPS spectra of the starting materials only show signals due to Fe^{3+} and SO_4^{2-}. The Fe 2*p* XPS signal of $Fe_2(SO_4)_3$ is 1.6 eV higher than that of hematite, which reflects the different chemical state of these compounds: $Fe_2(SO_4)_3$ is a salt, i.e. an ionic compound, while Fe_2O_3 is mainly covalent. The resulting pyrite phases are rather well defined, i.e. signals due to Fe^{2+} and S_2^{2-} are the main components of the respective XPS spectra. However, small contributions due to Fe^{III}–O (711.4 ± 0.3 eV) and polysulfide or neutral sulfur (165.0 ± 0.3 eV) can also be seen. The fact that both compounds convert into pyrite upon sulfidation is fully in line with the observations of the sulfidation behavior of surface-oxidized mackinawite samples and confirms the conclusion that the formation of pyrite from mackinawite requires a significant amount of oxidized species.

4. Discussion

The material presented in this manuscript combines experimental and quantum chemical work. We investigated structural and thermochemical properties of the reaction of mackinawite (Fe–S) with gaseous H_2S in comparison with phase transitions of mackinawite in inert gas. A phase diagram of homogeneous Fe–S reactions (solid solutions or aqueous solutions) in the compositional limits FeS to FeS_2 and in the temperature range from 0 to 350 °C has been published by Craig and Scott [41]. Their phase diagram includes a variety of stable and metastable phases, some of which are only ill defined, i.e. there are no reliable X-ray crystallographic data published. Important and sufficiently accurate determined phases are mackinawite (FeS), troilite (FeS), pyrrhotite (a variety of different compounds among them the hexagonal phases Fe_9S_{10} and Fe_7S_8), smythite (Fe_9S_{11}), greigite (Fe_3S_4), gamma iron sulfide (γ-Fe_2S_3), marcasite (FeS_2) and pyrite (FeS_2). Since our investigation addresses the heterogeneous reaction of solid mackinawite with gaseous H_2S, phase occurrences and relations as indicated in the above-mentioned phase diagram may be different in our case.

Phases of importance to our study are those shown in Fig. 1. Our DFT calculations show that the transitions of mackinawite to the phases of roughly the same stoichiometry (the hexagonal pyrrhotite phases Fe_9S_{10} and Fe_7S_8) are endothermic, whereas reactions with H_2S to phases of higher S:Fe ratios (greigite, $FeS_{1.333}$; marcasite and pyrite, FeS_2) are exothermic. Interestingly DFT calculates greigite as the compound of highest thermochemical stability. This result is in disagreement with experimental data where pyrite is clearly the most stable compound in the FeS–FeS_2 series of phases. As already mentioned above, there are certain problems with electronic structure calculations of magnetic compounds by means of DFT-based techniques, which may lead to exaggerated energies of formation [29]. Moreover, our calculations are performed for the ideal Fe_3S_4 stoichiometry as obtained from X-ray structural data [25], whereas greigite forms within solution mostly in a less-defined state. Nevertheless, the increased stability of greigite relative to mackinawite is in line with experimental data and can qualitatively be understood on structural chemical grounds. The mackinawite–greigite transformation consists essentially in a rearrangement of Fe atoms in a close-packed cubic array of S atoms, which is common to both phases, leading to a more efficient packing and a reduction of the cell volume by 12%, which represents a substantial enthalpic stabilization because of the overall increase of density [42]. The rearrangement is due to oxidation of two-thirds of the Fe atoms from Fe^{II} to Fe^{III}, which then occupy octahedral holes in the inverse spinel structure of greigite [1]. Our experiments, however, show that only surface-oxidized mackinawite reacts with H_2S to the exothermic phases greigite and pyrite, whereas non-oxidized

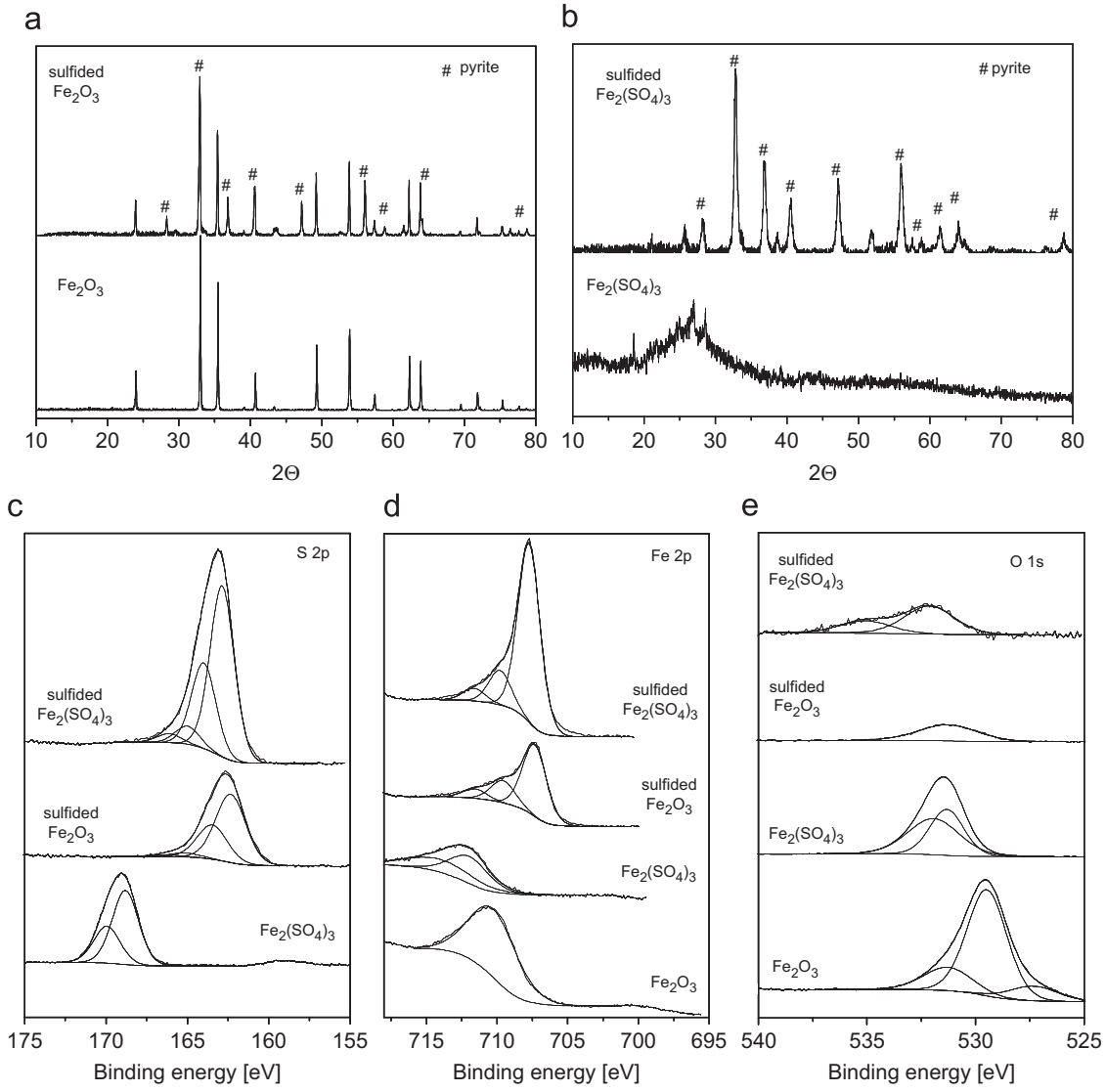

Fig. 8. XRD patterns (a, b) and Fe 2*p*, S 2*p* and O 1*s* XPS spectra (c–e) of Fe_2O_3 and $Fe_2(SO_4)_3$ as well as their products after reaction with H_2S at 300 °C for 6 h.

Table 7
Binding energies in the S 2*p* and Fe 2*p* XPS spectra of Fe_2O_3 and $Fe_2(SO_4)_3$ as well as their products after reaction with H_2S at 300 °C for 6 h as shown in Fig. 8

Species	Fe_2O_3	$Fe_2(SO_4)_3$	Sulfided Fe_2O_3	Sulfided $Fe_2(SO_4)_3$
S_2^{2-}			162.3	162.7
S_0/S_n^{2-}			165.1	165.0
SO_4^{2-}		168.7		
Fe^{II}–S			707.1	707.5
Fe^{III}–S			711.4	711.4
Fe^{III}	710.4	712.0		

Binding energies are accurate within ±0.3 eV.

mackinawite stays in the range of the endothermic $Fe^{2+}S^{2-}$ pyrrhotite phases.

The most important experimental findings of our study can be summarized as follows:

1. Upon thermal treatment in He or reaction with H_2S, non-oxidized mackinawite converts into pyrrhotite phases ($FeS \rightarrow Fe_9S_{10} \rightarrow Fe_7S_8$). The major measurable difference between the two reaction environments is the conversion temperatures, which are lower in the case of H_2S.
2. The surface of mackinawite is very sensitive to O_2. Oxidation experiments conducted under controlled conditions with synthetic air (5% O_2 in He) showed that first Fe^{2+} is oxidized to Fe^{3+} and, only if this process is completed, sulfide is oxidized to sulfate.
3. The state of surface oxidation of mackinawite determines the course of its reaction with H_2S. In the case of minor surface oxidation (only Fe^{2+} oxidized to Fe^{3+}) greigite forms. A similar reaction can be observed in inert gas atmosphere as well. Mackinawite that was oxidized under severe conditions (Fe^{2+} oxidized to Fe^{3+} and S^{2-} to SO_4^{2-}) converts into pyrite. Incomplete sulfidation leads to dependence of the extent of surface oxidation or sulfidation time to phase mixtures, i.e. greigite/pyrrhotite or pyrrhotite/pyrite.

Non-oxidized mackinawite converts into hexagonal pyrrhotite upon thermal treatment in He or H_2S. This phase transformation requires changing the sulfur sublattice from cubic closest to

hexagonal closest packing and the Fe coordination from fourfold to sixfold. To achieve this, all four Fe–S bonds in mackinawite must be broken [43]. The change of the sulfur sublattice transforms the layered structure of mackinawite to the three-dimensional NiAs-type structure of hexagonal pyrrhotite. If the surface of mackinawite bears structural and compositional deviations from its original state, such as in the case of minor (<20%) surface oxidation, the structural transformation is retarded, due to the presence of oxidized surface species, such as Fe^{II}–O and Fe^{III}–O (spectra I, Fig. 2). In H_2S atmosphere, Fe^{2+} centers in such oxidic environments react back to their sulfidic state with H_2S:

$$Fe^{II}-O + H_2S \rightarrow Fe^{II}-S + H_2O \quad (6)$$

Oxidic Fe^{3+} are also converted into sulfidic Fe^{II} by an oxygen–sulfur exchange reaction and a subsequent metal–ligand redox process:

$$Fe^{III}-O + H_2S \rightarrow Fe^{III}-S + H_2O \quad (7)$$

$$2Fe^{III}S \rightarrow Fe^{II}(S_2)Fe^{II} \quad (8)$$

Reactions (6)–(8) are well-known reactions to occur in the preparation of heterogeneous sulfide catalysts. These types of catalysts are typically prepared in the form of oxidic precursors and are then activated by converting the oxide into the respective sulfide by reaction with H_2S or gas mixtures containing H_2S [13,14]. The molecular mechanism of such sulfidation reactions and oxide–sulfide phase transitions were in detail investigated by Weber et al. [44] and van der Vlies et al. [45,46]. Although these studies deal with the sulfidation of molybdenum and tungsten oxides, the results can be applied to iron oxide–sulfide conversions as well, because of similarities in the structural chemical properties, redox potentials and the chemical hardness. In conclusion, H_2S facilitates the mackinawite–pyrrhotite phase transition in case of a slightly oxidized mackinawite surface. For reactions of mackinawite with H_2S to phases of higher S:Fe stoichiometries, the mackinawite surface must contain significant amounts of oxidized species.

Our experiments with surface-oxidized mackinawite show that surface Fe^{3+} centers are necessary for the formation of the Fe^{II}/Fe^{III} mixed-valence thiospinel compound greigite, while the formation of pyrite also requires oxidation of surface S^{2-} to SO_4^{2-}. The transition of mackinawite (FeS) into greigite ($Fe_3S_4 \equiv FeS_{1.333}$) or pyrite ($FeS_2$) goes along with an increase of the S:Fe stoichiometry, for which a source of sulfur must be available. This explains why pyrite cannot form within a heat treatment of surface-oxidized mackinawite in inert gas. For the same reason one might expect that surface-oxidized mackinawite can also not convert into greigite in He atmosphere. Our *in situ* XRD studies, however, clearly show that mackinawite converts gradually into greigite between 120 and 170 °C (Fig. 5). This transition involves the following changes in the oxidation states of Fe and in the S:Fe stoichiometry:

$$Fe^{II}S \rightarrow Fe^{II}Fe^{III}{}_2S_4 \quad (9)$$

$$FeS \rightarrow FeS_{1.333} \quad (10)$$

As a consequence, the mackinawite–greigite transition cannot be stoichiometric, because at an outside estimate three quarters of the Fe atoms of FeS can take part in the reaction to greigite. For reasons of stoichiometry and charge balance, the remaining Fe atoms must be present in an environment with a significantly lower S:Fe ratio than mackinawite and with Fe in a formal oxidation state less than 2+. Since there are no other phases next to greigite visible in the XRD patterns, not very much can be said regarding composition or structure of additional phases. On chemical grounds it is conceivable that the Fe atoms could either be present as elemental iron or in the form of substoichiometric iron oxides, the latter being more likely in view of our XPS data. The reason for the formation of greigite under these conditions lies in the thermochemical stability of the thiospinel structure. Greigite formed under these conditions is stable until 230 °C. Further heating leads to gradual transformation to pyrrhotite, the formation of which is completed at 290 °C (Fig. 5b). This process involves a slight change in the sulfur sublattice, a geometrical and electronic redistribution of Fe centers as well as restoring all Fe atoms back into one phase. The transition sequence mackinawite → greigite → pyrrhotite involves an increase and subsequent decrease of the S:Fe ratios and is thus surprising but nevertheless unequivocally demonstrated in our *in situ* XRD measurements.

The overall behavior of surface-oxidized mackinawite in inert gas is the same as that of non-oxidized mackinawite, which also converts into a pyrrhotite phase (hexagonal Fe_7S_8) at around 300 °C (*vide supra*). The mechanisms, however, are different. As discussed above, the non-oxidized sample stays in the regime of $Fe^{II}S^{2-}$-type phases and transforms into the hexagonal Fe_7S_8 pyrrhotite phase via Fe_9S_{10} as intermediate phase.

The sulfidation reactions of mackinawite with different degrees of surface oxidation are different, as shown in the XRD patterns and XPS spectra of Figs. 6 and 7. Here the extent of surface oxidation determines the course of the reactions as well as the sulfidation products. Mackinawite samples oxidized in synthetic air for 2 min contain Fe^{2+} and Fe^{3+}, but no SO_4^{2-} (spectra II, Fig. 2). Such samples react at 300 °C in H_2S to a mixture of greigite and pyrrhotite (pattern I, Fig. 6a). Pyrrhotite forms most likely in the same manner as discussed above for non-oxidized mackinawite samples, whereas greigite forms to that extent as Fe^{3+} is available to build up the mixed-valence thiospinel structure. Oxidation of mackinawite under more severe conditions (2 h) generates next to significant concentrations of surface Fe^{3+} also SO_4^{2-} (spectra III, Fig. 2). Sulfidation of this sample at 300 °C leads to a mixture of pyrite and pyrrhotite (pattern II, Fig. 6), where pyrrhotite again forms within a pure phase transition. Interestingly, greigite does not form, although Fe^{3+} was present in sufficient amounts. However, the conclusion that greigite does not form if the initial mackinawite sample contains SO_4^{2-} next to Fe^{3+} cannot be drawn, since the same preoxidized mackinawite sample converts into a mixture of greigite and pyrrhotite upon sulfidation at 150 °C (pattern III in Fig. 7). This means that greigite is stable at 300 °C in H_2S only at low initial mackinawite redox potentials. This leads to the conclusion that the extent of surface oxidation of the mackinawite surface does not only have an influence on the reaction pathway as already mentioned above, but also on the thermal stabilities of intermediate phases.

Full conversion of mackinawite to pure pyrite requires rigorous oxidation, since S^{2-} must stoichiometrically be oxidized to S_2^{2-}. Our XPS measurements show that those mackinawite samples that react with H_2S to pyrite contain Fe^{III}–O and SO_4^{2-} surface species. The surface of these mackinawite samples can to a certain extent be described by Fe_2O_3 and $Fe_2(SO_4)_3$, which both fully convert into pyrite upon sulfidation (Fig. 8).

Acknowledgments

We thank Mr. Gijsbert Gerritsen (Eindhoven University of Technology) for his help in the preparation of mackinawite and Dr. Huub Kooijman (Shell Research and Technology Centre Amsterdam) for the *in situ* XRD measurements. We gratefully acknowledge the National Research School Combination Catalysis Controlled by Chemical Design (NRSC-Catalysis) as well as the Royal Dutch Academy of Arts and Sciences for financial support.

References

[1] D. Rickard, G.W. Luther III, Chem. Rev. 107 (2007) 514.
[2] D.J. Vaughan, J.R. Craig, Mineral Chemistry of Metal Sulfides, Cambridge University Press, Cambridge, 1978.
[3] J.B. Corliss, J.A. Baross, S.E. Hoffman, Oceanol. Acta 4 (1981) 59.
[4] G. Wächtershäuser, Syst. Appl. Microbiol. 10 (1988) 207.
[5] G. Wächtershäuser, Microbiol. Rev. 52 (1988) 452.
[6] M.J. Russell, A.J. Hall, J. Geol. Soc. London 154 (1997) 377.
[7] G. Wächtershäuser, Philos. Trans. R. Soc. B 361 (2006) 1787.
[8] K.G. Cox, Nature 342 (1989) 342, 873.
[9] R.S. White, D.P. McKenzie, Geophys. Res. 94 (1989) 7685.
[10] E. Drobner, H. Huber, G. Wächtershäuser, D. Rose, K.O. Stetter, Nature 346 (1990) 742.
[11] Q. Wang, J.W. Morse, Mar. Chem. 52 (1996) 99.
[12] P. Taylor, T.E. Rummery, D.G. Owen, J. Inorg. Nucl. Chem. 41 (1979) 595.
[13] Th. Weber, R. Prins, R.A. van Santen, Transition Metal Sulphides, Chemistry and Catalysis, NATO ASI Series 3 High Technology, Kluwer Academic Publishers, Dordrecht, Netherlands, 1998.
[14] H. Topsøe, B.S. Clausen, F.E. Massoth, in: J.R. Anderson, M. Boudart (Eds.), Hydrotreatment Catalysis, Science and Technology, vol. 11, Springer, Berlin, 1996.
[15] H. Ohfuji, D. Rickard, Earth Planet. Sci. Lett. 241 (2006) 227.
[16] B. Delley, J. Chem. Phys. 92 (1990) 508.
[17] B. Delly, J. Chem. Phys. 113 (2000) 7756.
[18] M.D. Segall, P.J.D. Lindan, M.J. Probert, C.J. Pickard, P.J. Hasnip, S.J. Clark, S.C. Payne, J. Phys. Condens. Matter 14 (2002) 2717.
[19] J.P. Perdew, K. Burke, Y. Wang, Phys. Rev. B 54 (1996) 16533.
[20] S. Boursiquot, M. Mullet, M. Abdelmoula, J.-M. Génin, J.-J. Erhard, Phys. Chem. Miner. 28 (2001) 600.
[21] A.R. Lennie, S.A.T. Redfern, P.F. Schofield, D.J. Vaughan, Mineral. Mag. 59 (1995) 677.
[22] H.E. King, C.T. Prewitt, Acta Crystallogr. B 38 (1982) 1877.
[23] J.M.D. Coey, H. Roux-Buisson, Mater. Res. Bull. 14 (1979) 711.
[24] F. Keller-Besrest, G. Collin, Acta Crystallogr. B 39 (1983) 296.
[25] B.J. Skinner, R.C. Erd, F.S. Grimaldi, Am. Mineral. 49 (1964) 543.
[26] G. Brostigen, A. Kjekshus, C. Romming, Acta Chem. Scand. 24 (1970) 1925.
[27] P. Bayliss, Am. Mineral. 74 (1989) 1168.
[28] W.W. Barker, T.C. Parks, Geochim. Cosmochim. Acta 50 (1986) 2185.
[29] P. Raybaud, G. Kresse, J. Hafner, H. Toulhoat, J. Phys. Condens. Matter 9 (1997) 11085.
[30] D. Hobbs, J. Hafner, J. Phys. Condens. Matter 11 (1999) 8197.
[31] D. Rickard, Geochim. Cosmochim. Acta 70 (2006) A533.
[32] D. Rickard, A. Griffith, A. Oldroyd, I.B. Butler, E. Lopez-Capel, D.A.C. Manning, D.C. Apperley, Chem. Geol. 235 (2006) 286.
[33] A.R. Pratt, H.W. Nesbitt, I.J. Muir, Geochim. Cosmochim. Acta 56 (1994) 1.
[34] T.A. Patterson, J.C. Carver, D.E. Leyden, D.M. Hercules, J. Phys. Chem. 80 (1976) 1702.
[35] M. Mullet, S. Boursiquot, M. Abdelmoula, J.-M. Génin, J.-J. Erhard, Geochim. Cosmochim. Acta 66 (2002) 829.
[36] J.C. Muijsers, Th. Weber, R.M. van Hardeveld, H.W. Zandbergen, J.W. Niemantsverdriet, J. Catal. 157 (1995) 698.
[37] A.R. Pratt, H.W. Nesbitt, I.J. Muir, Geochim. Cosmochim. Acta 48 (1994) 5147.
[38] H.W. Nesbitt, I.J. Muir, Geochim Cosmochim Acta 58 (1994) 4667.
[39] J.R.B. Herbert, S.G. Benner, A.R. Pratt, D.W. Blowes, Chem. Geol. 144 (1998) 87.
[40] A.R. Lennie, K.E.R. England, D.J. Vaughan, Am. Mineral. 80 (1995) 960.
[41] J.R. Craig, S.D. Scott, in: P.H. Ribbe (Ed.), Reviews in Mineralogy, vol. 1, Mineralogical Society of America, Chelsea, 1974 (Chapter 5).
[42] A.R. Lennie, A.A.T. Redfern, P.E. Champness, C.P. Stoddart, P.F. Schofield, D.J. Vaughan, Am. Mineral. 82 (1997) 302.
[43] A.R. Lennie, K.E.R. England, D.J. Vaughan, Am. Mineral. 80 (1995) 960.
[44] Th. Weber, J.C. Muijsers, J.W. Niemantsverdiet, J. Phys. Chem. 99 (1995) 9194.
[45] A.J. van der Vlies, G. Kishan, J.W. Niemantsverdriet, R. Prins, Th. Weber, J. Phys. Chem. B 106 (2002) 3449.
[46] A.J. van der Vlies, R. Prins, Th. Weber, J. Phys. Chem. B 106 (2002) 9277.